EARTH'S CRYOSPHERE
SCIENTIFIC JOURNAL

Earth's Cryosphere, 2021, vol. XXV, No. 5, pp. 23–35 http://earthcryosphere.ru/

SNOW COVER AND GLACIERS

MASS BALANCE MODELLING FOR THE SARY-TOR GLACIER (THE AK-SHYIRAK MASSIF, INNER TIEN SHAN)

E.P. Rets[1], D.A. Petrakov[2], E.V. Belozerov[1], A.M. Shpuntova[2]

[1]*Water Problems Institute, RAS, Gubkina str. 3, Moscow, 119333, Russia; retska@mail.ru*
[2]*Lomonosov Moscow State University, Faculty of Geography, Leninskie Gory 1, Moscow, 119991, Russia*

As the direct measurements for the mass balance estimation can be applied only for a limited number of glaciers, alternative methods of estimation need to be developed. One of the most promising approaches is physically-based modelling, that is now being applied globally. In this study the mass balance of the Sary-Tor valley glacier was reconstructed for the period of 2003–2016. Originally developed for the North Caucasus AMelt model was modified to fit the conditions of continental glaciers. A block of snowpack processes was added to the model, including: head conductivity in the snowpack and in the active layer, water filtration in the snowpack and firn, congelation and regelation. The modelling results were verified using: 1) direct measurements on the ablation stakes net; 2) mass balance estimation according to geodetic method. The calibration parameters are compared to their measured values. Contrasting modeled mass-balance components for 2003–2016 and measured in 1985–1989 provided possibility to reveal climatically induced change of the Sary-Tor glacier dynamics.

Keywords: *mass balance modelling, glaciers, Tien Shan, AMelt model.*

INTRODUCTION

Glaciers are one of the key indicators of climate change and an important source of fresh water, especially in mountains surrounded by arid areas [*Kaser et al., 2010; Carey et al., 2017; McDowell et al., 2019*]. In Central Asia, the population of the foothills is highly dependent on water flowing from the mountains [*Lutz et al., 2013*]. The situation with freshwater resources is complicated by disputes between water-donor countries (Kyrgyzstan, Tajikistan) and water-consumer countries (Turkmenistan, Uzbekistan, and, to a lesser extent, Kazakhstan) [*Zhupankhan et al., 2017*]. The former are mainly interested in using water to generate electricity in the winter time, whereas the latter need water for irrigation farming in the summer. According to recent estimates, more than 20 million people in Kazakhstan, Turkmenistan, and Uzbekistan depend on irrigated agriculture [*Siegfried et al., 2012*].

Glaciers play a significant role in the runoff of the main rivers of Central Asia. According to [*Sorg et al., 2012*], more than two dozen studies are devoted to estimates of the contribution of glacial runoff to the river flow in Central Asia. On average, it is estimated at about 15 % for rivers of Kyrgyzstan. Glacial runoff is defined as the total runoff from the glacier, including water from melting ice, firn, and snow and rainwater runoff. The contribution of glaciers to river runoff increases by 1.5–3 times in summer, up to 50 % for the Amu Darya River, 27 % for the rivers of the Lake Issyk-Kul basin, and 80 % for the Tarym River. The contribution of glacial runoff to the Amu Darya River runoff is estimated at about 40 % in August and 25 % in July [*Armstrong et al., 2019*]. From the standpoint of the formation of river runoff, the widespread reduction in the area of the Tien Shan glaciers [*Narama et al., 2010; Bolch et al., 2019*] is still compensated by an increase in ablation [*Aizen et al., 2007; Huss, Hock, 2018*]. It is expected that the continuing reduction in the area of glaciation will lead to a decrease in river runoff in summer [*Sorg et al., 2012, 2014; Huss, Hock, 2018*]. Detailed studies of glaciers in Central Asia will make it possible to reduce the errors of scenarios of changes in water resources in the future [*Unger-Shayesteh et al., 2013; Sorg et al., 2014*] and will contribute to ensuring the water security of the region. Obviously, in order to predict correctly the evolution of glaciers, the detailed information on the response of glaciers to current and past climate changes is required [*Kronenberg et al., 2016*].

Such information can be provided both by direct observations of the mass balance and by modeling the mass balance of the glacier. After the collapse of the Soviet Union, all observations of the mass balance in the Tien Shan, Alai, and Pamir territories within the borders of the former USSR were curtailed (with the exception of Kazakhstan). They have been resumed only recently (https://wgms.ch). Mathematical modeling of the components of the mass balance of glaciers is used to solve a wide range of problems. There are models designed to carry out calculations on a

scale of whole mountain systems and for global generalizations [*Bliss et al., 2014; Huss, Hock, 2015, 2018; Shea, Immerzeel, 2016; Shannon et al., 2019*] and models with a more detailed description of the processes applicable to individual glaciers and glacial regions [*Klok, Oerlemans, 2002; Lehning et al., 2006; Ayala et al., 2017*]. Mathematical modeling was previously used to model the mass balance of individual glaciers in Kyrgyzstan – the Abramov Glacier [*Barandun et al., 2015*], Glacier no. 354 [*Kronenberg et al., 2016*], and the Suek West Glacier [*Kenzhebaev et al., 2017*]. The mathematical model of the Sary-Tor glacier was constructed in [*Rybak et al., 2019*] to carry out numerical experiments in order to study the possible evolution of glacier characteristics under different scenarios of climate change.

Reconstruction of the mass balance of the Sary-Tor Glacier for various periods was previously carried out on the basis of the relationship between the mass balance and the Equilibrium line altitude (ELA) [*Ushnurtsev, 1991; Mikhalenko, 1993*], as well as on the empirical dependences of the mass balance components on meteorological predictors [*Popovnin et al., 2021*].

The objectives of this study are: (1) to construct the mass balance model of the Sary-Tor Glacier (Ak-Shiyrak massif, Inner Tien Shan), basing on the spatially distributed energy-balance AMelt model [*Rets et al., 2011*]; (2) to reconstruct the glacier mass balance for 2003/04 to 2015/16 balance years; (3) to verify the results of modeling using in-situ data and geodetic mass balance, and (4) to analyze changes in the mass balance of the glacier in comparison with the period of 1985–1989 [*Dyurgerov, 1995*].

STUDY AREA

The Sary-Tor Glacier is a valley glacier in the upper reaches of the Naryn River within the Ak-Shyirak massif. In 2018, the glacier area was 2.63 km^2 (Fig. 1) [*Shpuntova et al., 2019*]. The Ak-Shiyrak massif is characterized by a continental climate, which is mainly manifested in the frequent recurrence of air masses of the continental type and a small amount of atmospheric precipitation. In the annual distribution of precipitation, the summer maximum is well pronounced: on average, 70–80 % of the annual precipitation fall from May to September [*Dyurgerov, 1995*]. The mean annual precipitation according to records of the nearest Kumtor weather station (3659 m a.s.l.) is 317 mm [*Petrakov et al., 2016*]. At altitudes of about 4000 m, more than 90 % of the annual precipitation is in the solid form [*Voloshina, 1988*].

The Sary-Tor Glacier was recognized as a reference glacier for the Ak-Shiyrak massif and was the object of mass balance monitoring in 1985–1991. In 2014, the mass balance measurements on the Sary-Tor Glacier were resumed by the Institute of Water Problems and Hydropower of the National Academy of Sciences of Kyrgyzstan.

METHODS AND INITIAL DATA

Brief description of modeling approaches

To model the mass balance of the Sary-Tor glacier, the AMelt model of snow and ice melting in alpine basins was used. This energy-balance model with distributed parameters was suggested by E.P. Rets with co-authors [*2011*]. It implies the solution of the

Fig. 1. Location of the Sary-Tor Glacier, other considered glaciers, and the Kumtor weather station.

energy balance equation at each point of the computational grid:

$$-\omega = (S_b + S_{df})(1 - A) + E_{lrd} - E_{lru} \pm$$
$$\pm H \pm LE \pm Q_m \pm Q_{snp} \pm Q_{act},$$

where ω is the energy balance of the surface, W/m^2; S_b, S_{df} is the incoming direct and diffuse short-wave radiation, respectively, W/m^2; A is the surface albedo; E_{lrd} is the counter radiation of the atmosphere, W/m^2; E_{lru} is the long-wave radiation of the earth's surface, W/m^2; H is the sensible turbulent heat exchange with the atmosphere, W/m^2; LE is the latent turbulent heat exchange with the atmosphere, W/m^2; Q_m is the heat flux through the debris cover, W/m^2; Q_{snp} is the energy change due to processes in the snowpack and at the snow/ice interface, W/m^2; and Q_{act} is the energy change due to processes in the active layer of ice and firn, W/m^2.

All calculated values are distributed over the cells of a regular grid.

To separate the incoming short-wave radiation (S_g) into direct (S_b) and diffuse (S_{df}) radiation, the following dependency [*Bindi et al., 1992; Boland, Ridley, 2008*] is used:

$$S_{df}/S_b = f(k),\ k = S_g/S_o,$$

where k is the transparency coefficient of the atmosphere, and; S_o is the shortwave radiation at the upper boundary of the atmosphere.

The spatial distribution of the incoming short-wave radiation at a grid cell at each time point is based on:

– the angle of incidence of sun rays, calculated from the height of the sun above the horizon and the coordinates of the normal vector to the surface of the i-th elementary area centered at the grid cell;

– the angle of closure of the horizon by the surrounding relief of the surface of the i-th elementary area centered at the grid cell in the j-th sector of the horizon, corresponding to the current azimuth of the sun for each time step.

Diffuse solar radiation arriving at the surface of the i-th elementary area centered at the grid cell $\left(S_{df_i}\right)$ consists of diffuse short-wave radiation coming from the visible part of the sky and re-reflected from the surrounding area:

$$S_{df_i} = S_{df_0}\left(1-\overline{a}_i\right)+\overline{a}_i A_i'' S_{g_i}'',$$

where S_{df_0} is the scattered radiation flux at a fully open sky, W/m^2; $\overline{a}_i$ is the average proportion of the closure of the firmament by the surrounding relief on the i-th elementary area; A_i'' is the albedo of the surrounding area of the i-th elementary area; and S_{g_i}'' is the total short-wave radiation arriving at the surface of the i-th elementary area, W/m^2.

The albedo of the surface of the i-th elementary area is determined in accordance with the type of its surface. The albedos of melting snow, ice, firn and debris are set as constants based on field measurements and literature sources. In case of snowfall, the albedo increases to the albedo of fresh snow, then exponentially decreases to the albedo of melted snow, depending on the time elapsed since the last snowfall [*Rohrer, Braun, 1994*].

Long-wave surface radiation (E_{lru}) is calculated using the Stefan–Boltzmann equation. The counter radiation of the atmosphere (E_{lrd}) is calculated using the Angstrom formula. Turbulent heat exchange with the atmosphere (latent and sensitive heat fluxes) is calculated using the empirical formula of *P.P. Kuzmin* [*1961*].

The model was previously tested for the Djankuat and Bashkara glaciers (North Caucasus) [*Rets, Kireeva, 2010; Rets et al., 2011, 2014; Belozerov et al., 2020*] and the Grenfjord glacier (Spitsbergen) [*Elagina et al., 2021*]. Comparison of the simulation results with the results of direct observations on the network of ablation stakes attested to a good reproducibility of the results of field observations by the model.

The model was originally developed for the conditions of the North Caucasus [*Rets et al., 2011*] and had to be adapted for the climatic conditions of Central Asia. The model was supplemented with the blocks of water filtration through the snowpack and firn; water refreezing in the snowpack, at the snow/ice boundary, and in the firn; and the heat transfer in the active layer of the glacier. The snowpack in the design scheme was presented as a system of layers, between which the heat transfer and the gravitational filtration of water took place. Also, the calculation of melt water yield per unit area of the glacier was added.

In the modified version of the model, the snowpack is divided into layers. The snow layers have a fixed thickness h (specified in mm by the StepTprof parameter), except for the top layer, the thickness of which is variable: it increases with fresh snow falling and decreases with melting. If the increasing thickness of the top layer reaches the StepTprof value, another layer is added to the snowpack. If the thickness of the top layer becomes zero, the snowpack becomes reduced by one layer.

In this version of the AMelt model, the vertical precipitation gradient (dP, %/100 m), which is a calibrated parameter, is used to describe the spatial distribution of liquid precipitation. When precipitation falls at an air temperature of less than –2 °C, it is considered that precipitation falls in solid form at each point of the grid cell.

Each layer has a set of characteristics that are averaged for a given layer: T – temperature, °C;

c – heat capacity, J/(kg·°C); H_w – gravitational water content, mm; Θ_{vir} – capillary water content, mm; ρ_{sn} – snow density, g/cm^3; λ_{sn} – coefficient of molecular thermal conductivity of snow, W/(m·K).

The initial values of the snow density and the gravitational and capillary water contents are set the same for all snow layers, based on the available observation results, the archived data for adjacent areas and the theoretical concepts [*Konovalov, 1985; Singh, Singh, 2001; Seo et al., 2008*].

The heat capacity of snow is calculated from the heat capacity of ice, air and water in accordance with the density of snow and the content of gravitational and capillary water. The coefficient of thermal conductivity of the snow layer is calculated at each time step using its dependence on the density of snow [*Sturm et al., 1997*].

The initial temperature distribution in the snow stratum is set as uniform, equal to the mean air temperature for January–February.

In the extended version of the AMelt model, the change in the temperature of the snow layers occurs in the process of molecular heat transfer between the snow layers and heat release during the refreezing of infiltrated melt water into this layer.

1. Molecular thermal conductivity is calculated layer by layer as:

$$Q_{ij} = \lambda_{snij} (T_i - T_j)/dh,$$

where Q_{ij} is the heat flux due to molecular thermal conductivity between snow layers i and j, W/ m^2; λ_{snij} is the coefficient of thermal conductivity of snow averaged for layers i and j, W/(m·K) and given as a function of snow density [*Sturm et al., 1997*]; T_i is the temperature of the i-th layer of snow, °C; T_j is the temperature of the j-th layer of snow, °C; and dh is the distance between snow layers, m.

2. The release of heat inside the layer during the refreezing of infiltrating melt water into this layer (Q_{Lm}, W/m^2) is calculated as:

$$Q_{Lm} = Lm,$$

where L is the specific heat of fusion of ice ($3.335 \cdot 10^5$ J/kg); m is the mass of refreezing water, kg.

Infiltration is calculated from an adapted version of Darcy's law [*DeWalle, Rango, 2008; Snow..., 2008*]. The infiltration rate u_w is given as a function of the ρ_{sn}, the average grain diameter d, the proportion of gravitational water in the snow pores S_w, and the water-holding capacity Θ_{vi}:

$$u_w = f(\rho_{sn}, d, S_w, \Theta_{vi}).$$

The water-holding capacity of snow (in fractions of a unity) is calculated from its dependence on the porosity of the snow p [*Coleou, Lesaffre, 1998*]:

$$\Theta_{vi} = 0.057p/(1 - p) + 0.017.$$

The porosity of the snow is calculated approximately from the snow density as $(1 - \rho_{sn})$.

The density of the snow layer increases in the course of refreezing of infiltration water. In this case, the snow density is calculated at each step as:

$$\rho_{sn}^t = \left(\rho_{sn}^{t-1} h + 0.917\left(H_w^t + \Theta_{vir}^t\right)\right) \Big/ \left(h + H_w^t + \Theta_{vir}^t\right).$$

The density of the newly accumulated fresh snow layer is set by the RoFreshSnow parameter.

If the thickness of the top snow layer is less than 0.7 StepTprof, then it is combined with the underlying snow layer or with the surface ice layer (if this is the only snow layer) during the layer-by-layer calculation of thermal conductivity.

The active layer of the glacier is also divided into layers, the number of which is set by the nLIce model parameter. Heating/cooling of the active layer of ice proceeds due to molecular thermal conductivity; an additional source of thermal energy is the refreezing of water on the surface of ice at a temperature below the melting point. The initial temperature distribution in the active ice layer is linear: from the surface layer, the initial temperature of which is equal to the mean January–February temperature, to the bottom of the active layer with a constant temperature specified by the Tact parameter.

Water loss from the firn occurs after the cold content (*CC*) condition of the firn is satisfied [*Takeuchi et al., 2014*].

The filtration coefficient for describing the process of water filtration through the firn was adopted according to the published data of experimental measurements by various scientific groups [*Oerter, Moser, 1982*].

The modeled accumulation values include the total accumulation, as well as the refreezing of melt water in the snow stratum, on the ice surface, and in the firn layer. Avalanche feeding is not taken into account in this version, since it is practically absent for the object under study due to the features of the relief. Wind redistribution of solid precipitation is taken into account indirectly, considering the position of the firn line: for areas above the firn line of a given year, an additional coefficient is applied to the altitudinal increase in precipitation. For the Sary-Tor glacier, in the areas above the firn line, the value of precipitation additionally increases by 30 %.

Adaptation of the AMelt model for the Sary-Tor Glacier

The following input data were used to build a model of the Sary-Tor glacier:

1) a digital elevation model composed of a highly detailed model obtained for the surface of the Sary-Tor Glacier from a GeoEye stereoscopic pair (July 29, 2012) and an SRTM model for the surrounding landforms;

2) meteorological data with a 1 h resolution for 2003–2016 from the automatic weather station (AWS) Campbell located less than 5 km from the gla-

cier at the height of 3659 m asl, including incoming shortwave radiation (S_g, W/m^2), air temperature ($T(H)$, °C), wind speed (U, m/s), relative air humidity (e, %), and precipitation (P, mm) (provided by the Kumtor Gold Company);

3) the position of the firn line and glacier boundaries for each year as determined from Landsat images;

4) field data on melting regime as measured in 2015 on a network of ablation stakes was used for model calibration;

5) field data on melting regime as measured in 2014 on a network of ablation stakes was used for model validation.

In the model adapted for the Sary-Tor Glacier, the heat flux through the debris cover was not taken into account, since there is practically no debris cover on the glacier.

The albedo values of ice, firn, melted snow, and freshly fallen snow were taken as 0.25, 0.4, 0.55, and 0.8, respectively, according to the averaged results obtained by D.A. Petrakov with coauthors in the studied region [*Petrakov et al., 2019*].

As we had no data on air temperatures and precipitation, as well as on the snow depths at different heights during the modeled period, the altitudinal gradients of precipitation and air temperature were calibrated.

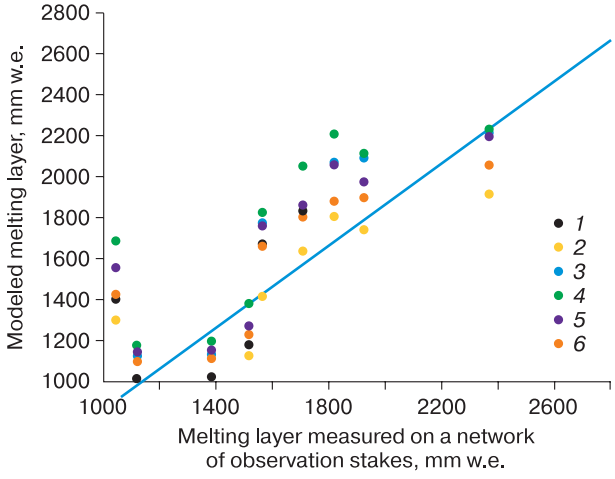

Fig. 2. Calibration of the Sary-Tor Glacier model according to the results of field measurements on a network of ablation stakes in 2015.

Blue line – linear approximation function. Results of model experiments with different values of calibration parameters of air temperature (*dP*, precipitation gradient; *dT*, temperature gradient; t_{sh}, temperature shift); *1* – dP = 20 %/100 m, dT = –7 °C/1000 m, t_{sh} = 0 °C; *2* – dP = 20 %/100 m, dT = –6 °C/1000 m, t_{sh} = 1 °C; *3* – dP = 20 %/100 m, dT = –5.5 °C/1000 m, t_{sh} = 0.5 °C; *4* – dP = 20 %/100 m, dT = –5 °C/1000 m, t_{sh} = 0.5 °C; *5* – dP = 20 %/100 m, dT = –5 °C/1000 m, t_{sh} = 0.75 °C; *6* – dP = 20 %/100 m, dT = –5 °C/1000 m, t_{sh} = 1 °C.

The best agreement of the model data with the field data for all altitudinal zones was obtained at a temperature gradient of –7 °C per 1000 m, a temperature shift equal to 0 °C, and a precipitation gradient of 20 % per 100 m. The choice of these parameters is analyzed in the Discussion section. In this case, the deviation of the simulated values from the measured values in different parts of the glacier may be associated with spatial differences in the temperature regime and the distribution of snow, which cannot be described by a constant gradient (Fig. 2).

The simulation results were validated using two independent methods:

1. Comparison of the results of modeling with the field data obtained in 2014, which demonstrated a good agreement between them (Fig. 3). The correlation coefficient was 0.99. The Nash-Sutcliffe model efficiency coefficient (NSE) for 2014 was 0.95 [*Garrick et al., 1978*]. A small systematic deviation was noted: the model overestimated the melting in the middle and lower zones of the glacier by about 0.05–0.1 m w.e. (meters of water equivalent).

2. Comparison of the change in the average surface height of the Sary-Tor Glacier from July 29, 2003 to September 29, 2013 as determined from the analysis of stereoscopic pairs of QuickBird and GeoEye satellite images [*Petrakov et al., 2016*] with the total modeled mass balance of the glacier for this period. The average decrease in the surface height was 3.8 m according to the geodetic method and 4.3 m according to the modeling. The deviation of the simulation results from the measured data was 13 % over the 10 mass balance years, or 0.05 m per year. Thus, we can say that the simulation by the AMelt model reliably represents the dynamics of the mass balance of the glacier.

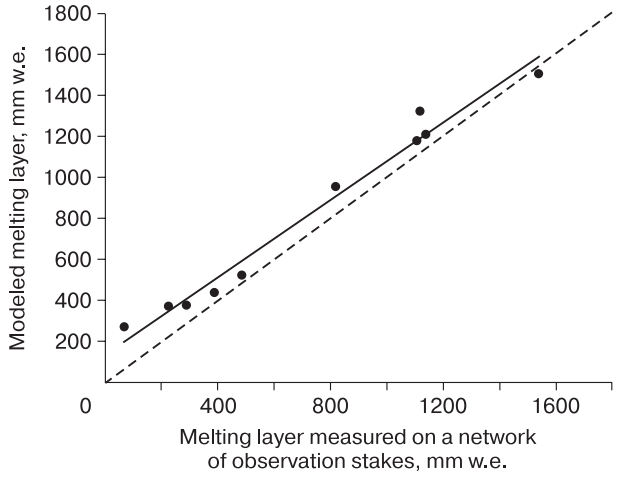

Fig. 3. Verification of the model based on the results of field observations on a network of ablation stakes on the Sary-Tor Glacier in 2014.

Dashed line: graph $y = x$; solid line: linear approximation function.

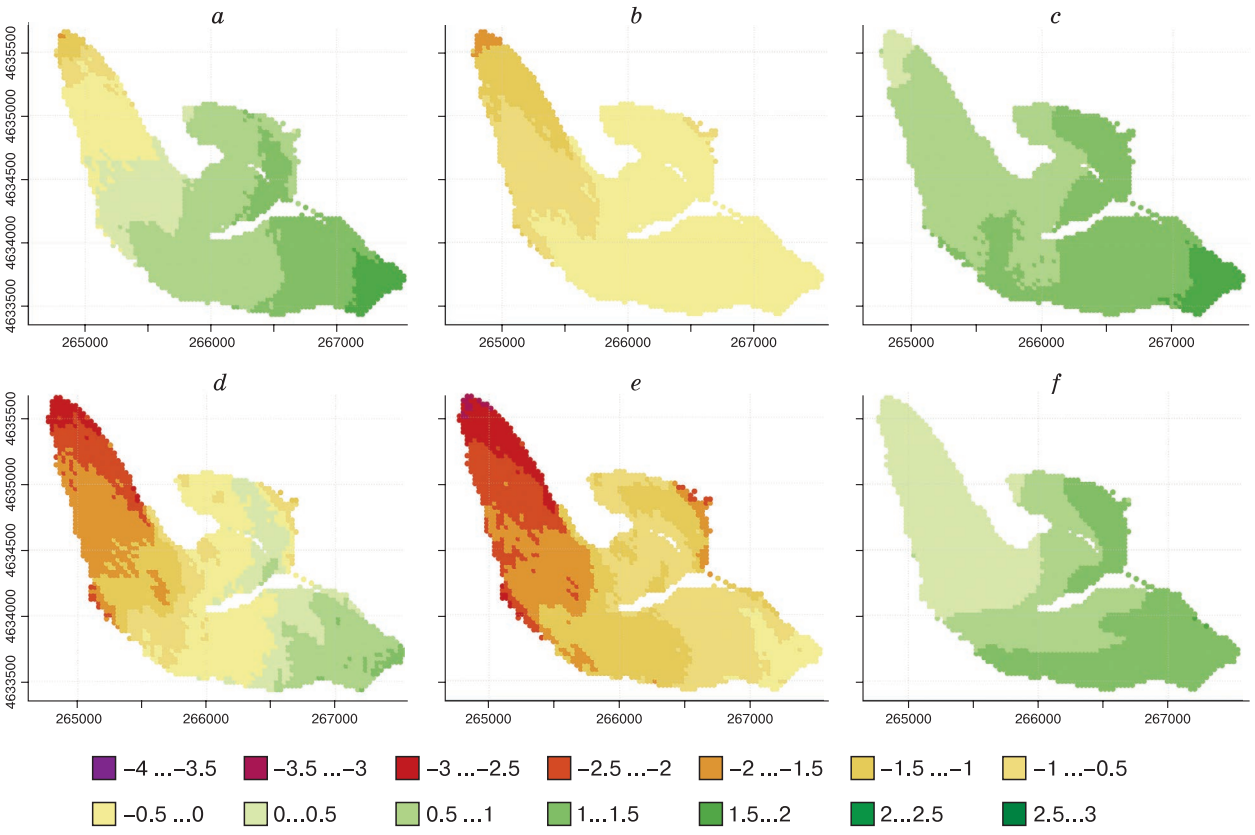

Fig. 4. Schematic maps of mass balance fields of the Sary-Tor Glacier for glaciological years of (*a*, *b*, *c*) 2008/09 and (*d*, *e*, *f*) 2014/15: (*a*, *d*) mass balance Bal; (*b*, *e*) surface lowering due to ablation Abl; and (*c*, *f*) accumulation Acc.

The color shows the change in the surface height, m w.e.

Table 1. **Annual values of the mass balance (Bal), ablation (Abl), and accumulation (Acc) of the Sary-Tor Glacier according to modeling data**

Mass balance year	Bal	Abl	Acc
	m w.e.		
2003/04	−0.44	1.03	0.59
2004/05	−0.52	0.99	0.48
2005/06	−0.71	1.24	0.54
2006/07	−0.47	1.09	0.62
2007/08	−0.63	1.10	0.46
2008/09	0.37	0.53	0.89
2009/10	−0.62	1.34	0.72
2010/11	−0.37	1.05	0.68
2011/12	−0.56	1.24	0.68
2012/13	−0.36	0.98	0.62
2013/14	−0.50	0.96	0.46
2014/15	−0.76	1.42	0.67
2015/16	−0.48	1.09	0.61
Average value	−0.463	1.08	0.618

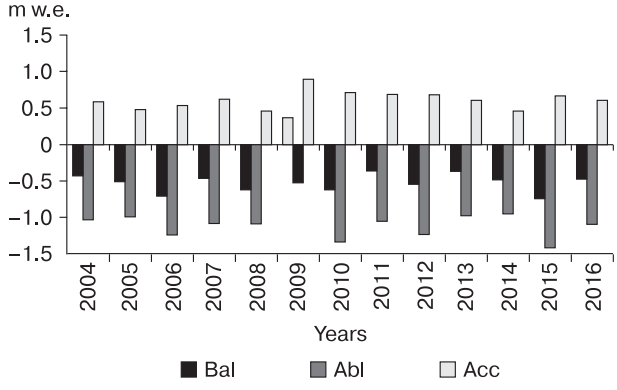

Fig. 5. Accumulation (Acc), change in the height of the glacier surface due to ablation (Abl), and mass balance (Bal) of the Sary-Tor Glacier for the period 2003/04–2015/16 according to the modeling.

RESULTS

The output of the model is the depth of snow, firn, and ice melt and corresponding water yield calculated for each point of the regular grid (30 × 30 m) at each time step (in this work, 1 h). Examples of the spatial distribution of the total values of ablation, accumulation, and mass balance of the Sary-Tor Glacier calculated for the mass balance year are shown in Fig. 4. According to the model, the annual accumulation on the Sary-Tor Glacier varies from 0.48 to 0.89 m w.e. in different years, and the ablation changes from 0.53 to 1.42 m w.e. (Table 1 and Fig. 5). For most of the years during the study period, the glacier mass balance is negative and averages –0.46 m w.e. per year. With regard to mass balance, the only positive year was 2009 because of the low ablation and increased accumulation.

DISCUSSION

Despite the fact that the AMelt model is focused on physically-based simulation of snow and ice melting, the lack of complete information about the simulated objects necessitates the use of calibration parameters: the gradients of temperature and precipitation in this case. The problem of the presence of calibration parameters in hydrological models has long been known and widely discussed [*Christophersen et al., 1990; Beven, Freer, 2001; Kirchner, 2006; Vinogradov, Vinogradova, 2010; Semenova, Beven, 2015*]. When calibrating, the modeler strives to achieve, first of all, the correspondence of the main sought parameter (in the case of hydrological modeling, the runoff in the outlet; in the case of glaciological modeling, the final mass balance) to the observational data. It is important that the same satisfactory result can be obtained using different independent sets of values, i.e., calculations with different initial values in hydrological modeling are equifinal. Moreover, the values of the calibration parameters can go beyond their physical limits for a given object and lose their physical meaning. Accordingly, in the course of model calibration, the mechanisms of the simulated process can be significantly distorted.

In accordance with this, the authors consider it appropriate to analyze the selected values of the calibration parameters (see the Methods and data section), as well as the results of modeling individual components of the dynamics of the Sary-Tor Glacier mass balance, for which observational data can be found for comparison.

The altitudinal temperature gradient was taken equal to –7 °C per 1000 m, and the altitudinal precipitation gradient was 20 % per 100 m. The representation of the vertical distribution of air temperature and precipitation as a linear function with a constant slope is a significant simplification. In reality, the vertical distribution of these parameters in the mountains is not described by a linear function; it is strongly affected by local factors and changes significantly both during the entire season and during one day [*Barry, 2008*].

The results of simultaneous observations over the air temperature at the Tien Shan weather station (it was located in the same trough valley as the modern Kumtor weather station, 9 m lower) and in the middle part of the ablation zone on the Davydov Glacier (which occupies the neighboring valley) in July–August 1984 were presented in the study by *A.P. Voloshina* [*1988*]. In summer, during the daytime in clear weather, the air temperature at the weather station can exceed the air temperature in the middle part of the ablation zone on the glacier by 4–6 °C, while temperature inversions are usually observed at night. On average, the recorded difference in air temperatures between the two points was 1.6–2.6 °C, which corresponded to a temperature gradient of 5.5–8.9 °C per 1000 m; on average, –7.2 °C per 1000 m. This value turned out to be extremely close to the calibration parameter of the temperature gradient, which gave the best fit of the simulated melting to the results of factual measurements at the Sary-Tor Glacier.

The work [*Voloshina, 1988*] also contained data on simultaneous measurements of precipitation at the same points. The magnitude of the precipitation gradient, according to the observation results, depended on the amount of precipitation at the height of the weather station: with an increase in the amount of precipitation, the gradient decreased exponentially, settling at a level of 25–30 % per 100 m with the amount of precipitation equal to 3 mm or more.

Thus, the precipitation gradient adopted in the model (20 % per 100 m) may be somewhat underestimated, but it is close to the values typical for this region.

The altitudinal distribution of solid precipitation on a glacier is determined by a combination of the altitudinal distribution of liquid precipitation and air temperature.

According to [*Dyurgerov et al., 1992*], the altitudinal gradient of solid precipitation during summer snowfalls in 1987–1989 was variable. It usually increased with an altitude from 0–20 % per 100 m in the lower glacier zones to 40–100 % per 100 m at the height of 4200–4400 m a.s.l., and decreased to 10–40 % at the heights above 4400 m a.s.l. The average value of the altitudinal gradient of solid precipitation was 46 % per 100 m. The simulated altitudinal distribution of annual precipitation and accumulation is relatively even because of constant temperature and precipitation gradients: the accumulation gradients increase from 20–40 to 40–100 % per 100 m; this

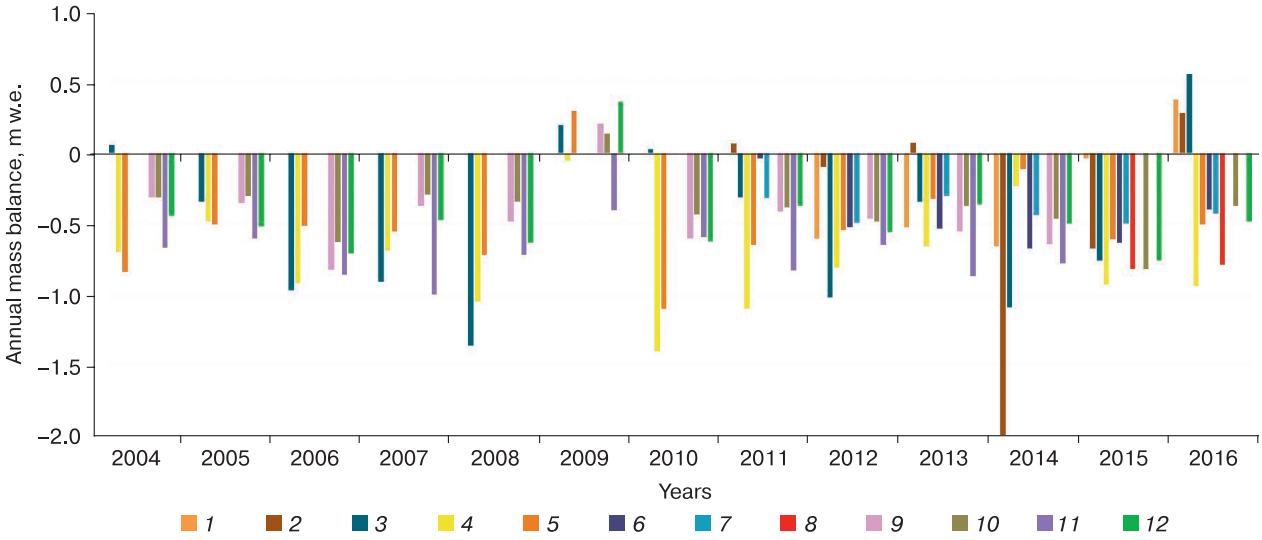

Fig. 6. Annual values of the mass balance on the Tien Shan glaciers in the period from 2003/04 to 2015/16 balance years.

According to the glaciological method (https://wgms.ch/): *1* – Abramov Gl, *2* – Golubev Gl, *3* – Tuyuksu Gl, *4* – Glacier no. 1 Urumqi, eastern branch; *5* – Glacier no. 1 Urumqi, western branch; *6* – Glacier no. 354; *7* – Western Suek Gl, and *8* – Sary-Tor Gl. Mass balance reconstruction: *9* – Glacier no. 354 [*Kronenberg et al., 2016*], *10* – Western Suek Gl [*Kenzhebaev et al., 2017*], *11* – Sary-Tor Gl [*Popovnin et al., 2021*], and *12* – Sary-Tor Gl (present study).

gradient decreases at the altitude above 4400 m. The average simulated accumulation gradient is 52 % per 100 m. It can be stated that the model simplifies the real field of snow distribution due to the simplified consideration of the vertical distribution of temperature and precipitation.

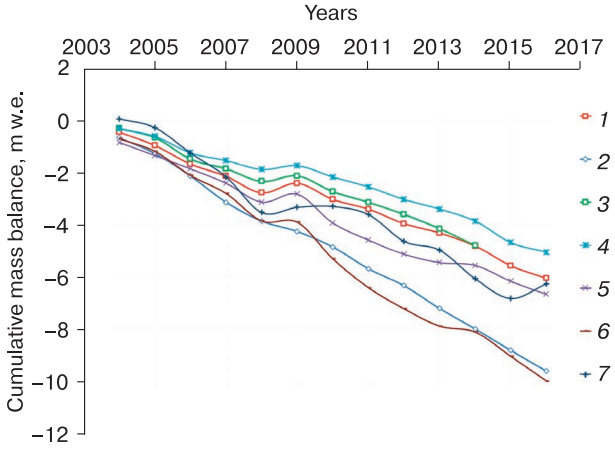

Fig. 7. Comparison of cumulative mass balance curves for Tien Shan glaciers.

According to modeling data: *1* – Sary-Tor Gl (present work); *2* – Sary-Tor Gl (reconstruction based on empirical dependences on meteorological predictors [*Popovnin et al., 2021*]); *3* – Glacier no. 354 [*Kronenberg et al., 2016*]; *4* – Western Suek Gl [*Kenzhebaev et al., 2017*]. According to the glaciological method (https://wgms.ch/): *5* – Glacier no. 1 Urumqi, western branch; *6* – Glacier no. 1 Urumqi, eastern branch; and *7* – Tuyuksu Gl.

According to the modeling data, the mass balance of the Sary-Tor Glacier in 2004–2016 repeated the trends observed on the Tien Shan glaciers according to the data of direct observations and reconstructions by various authors (Figs. 6 and 7). For most of the glaciers, a positive mass balance was observed in 2009. The simulated annual mass balance values of the Sary-Tor Glacier fit into the range of measured and modeled elsewhere mass balance values of the Tien Shan glaciers (Fig. 6). The obtained annual values are closest to the measured and modeled values reported for the nearby glaciers no. 354 and Western Suek.

The mass balance of the Sary-Tor Glacier simulated for 2015 demonstrated a good agreement with the mass balance determined by the glaciological method (–0.76 and –0.82 m w.e., respectively). In 2016, the discrepancy between the simulated and factual (glaciological method) mass balances was 0.31 m w.e. (–0.48 and –0.79 m w.e., respectively). The differences may be associated primarily with the different methodology for extrapolating the values of the glacier mass balance to the area, for which observational data are absent, or with errors of both the glaciological method (estimated at about 0.2 m w.e. for this region [*Kronenberg et al., 2016; Kenzhebaev et al., 2017*]) and the modeling method. For the present model, the average error in calculating the annual balance is approximately 0.1 m w.e. (see the Results section). It should also be noted that the values of the modeled and experimentally determined mass ba-

lance of the Sary-Tor Glacier in 2015 (–0.76 and –0.82 m w.e., respectively) are within the range of the mass balance values observed for most of the glaciers in the region (from –0.499 to –0.93 m w.e.), except for the Abramov Glacier with a mass balance close to zero in that year (*https://wgms.ch/*). In 2016, the loss of mass of glaciers in the region was less significant than in 2015: from –0.37 to –0.5 m w.e. (the exception was Urumqi, the eastern branch). For many glaciers, the mass balance was even positive (from 0.287 to 0.561 m w.e.) (*https://wgms.ch/*). Thus, the modeled value of the mass balance of the Sary-Tor Glacier for 2016 (–0.48 m w.e.) was closer to the regional distribution than that obtained by the glaciological method (–0.79 m w.e.).

In general, according to the obtained results, the mass of the Sary-Tor Glacier decreases slower than that of the Urumchi and Tuyuksu glaciers, and faster than that of the Western Suek Glacier. The cumulative curve obtained from the reconstruction of the mass balance of glacier no. 354 [*Kronenberg et al., 2016*] is the closest to the one obtained for the Sary-Tor Glacier.

Reconstruction of the mass balance of the Sary-Tor Glacier based on empirical relationships between the components of the mass balance and the meteorological predictors [*Popovnin et al., 2021*] demonstrated good agreement with the results of our modeling for 2005, 2006, 2008, 2010, and 2012. In other years, the values of the mass balance reconstructed from the empirical dependences on meteorological predictors were lower than those obtained with the help of the AMelt model (Fig. 6). As a consequence, the cumulative mass balance curve of the Sary-Tor Glacier obtained by the reconstruction method with the use of empirical dependences on meteorological predictors [*Popovnin et al., 2021*] lies significantly lower than the curve obtained in our study and closer to the curve obtained for the Tuyuksu Glacier (Fig. 7).

Comparison of the simulation results with observational data on the Sary-Tor Glacier in 1984/85–1988/89 [*Dyurgerov et al., 1992; Dyurgerov, 1995*] reveals the intensification of the glacier mass loss. The average value of the mass balance in the modern period (2003/04 to 2015/16) was –0.46 m w.e.; in 1984/85–1988/89, it was –0.14 m w.e. According to the reconstruction by *S.N. Ushnurtsev* [*1991*] based on the relationship between the mass balance and the height of the feeding boundary, the mass balance of the Sary-Tor Glacier in the period from 1930 to 1984 ranged from –0.6 to 0.2 m w.e. A similar tendency for the intensification of mass loss is observed for all Tien Shan glaciers provided with long-term observation series (Fig. 8).

The intensification of the loss of mass by the Sary-Tor Glacier occurred primarily due to the increased melting in the lower altitudinal zones. In the accumulation zone, the annual mass balance values

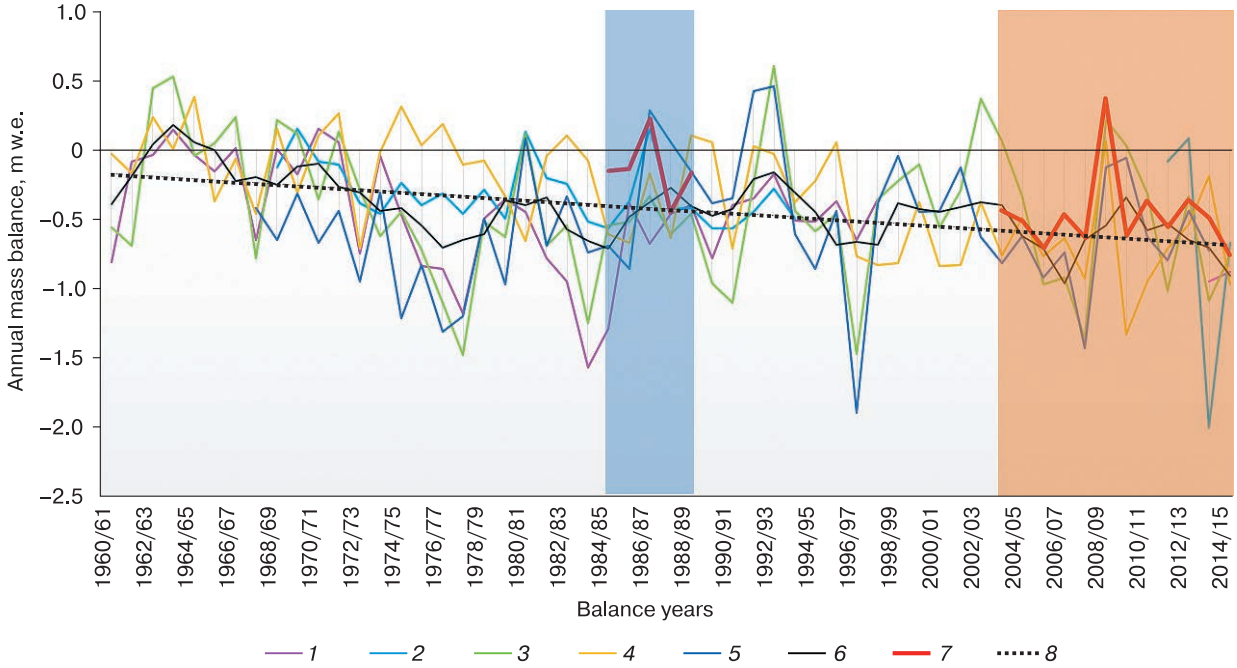

Fig. 8. Long-term fluctuations in the mass balance of the Tien Shan glaciers.

1 – Karabatkak Gl; *2* – Golubev Gl; *3* – Tuyuksu Gl; *4* – Urumqi Gl; *5* – Abramov Gl, *6* – moving average with a three-year window; *7* – Sary-Tor Gl (1984/85–1988/89, observation data [*Dyurgerov, 1995*]; 2003/04–2015/16, modeling data); *8* – linear approximation of a moving average with a three-year window. Graphs *1–5* are based on data from the Internet resource https://wgms.ch/.

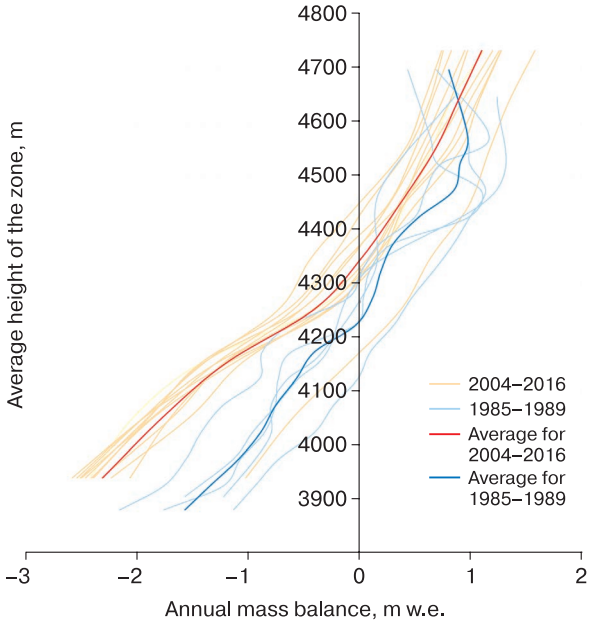

Fig. 9. Altitude distribution of the annual mass balance for the model period (2004–2016) and the period of field observations (1985–1989).

averaged over altitudinal zones for 1984/85–1988/89 and 2003/04–2015/16 are generally close: the ranges of variation coincide for both periods, and the average for the latter period is shifted towards more negative values by 0–0.25 m w.e. (Fig. 9). At the altitude below 4300 m asl, the averaged curves begin to diverge: at the altitudes of 3900–4000 m, melting in the recent period was 1.0–1.2 m w.e. higher than that in the 1980s. The ELA shifted upwards by 125 m: from 4225 m in 1984/85–1988/89 to 4350 m in 2003/04–2015/16 with a range of variation from 4254 to 4446 m.

A smoother pattern of the altitudinal distribution of the mass balance in the model period compared to the period of field observations in the 1980s is associated with a simplified representation of the altitudinal distribution of precipitation and temperature. Spatial differences in the structure of the modeled values of the glacier balance are due to the distribution of solar radiation and the surface topography (Fig. 10).

The intensification of the ablation of glaciers in the Ak-Shyirak massif occurs against the background of an increase in the annual and summer air temperatures (Fig. 11, *a*). Thus, the air temperature of the warm (May–September) season in 1984/85–1988/89 at the Tien Shan weather station was +1.8 °C; in 2003/04–2015/16, it increased to +3.0 °C. The rise in temperature was not offset by a significant increase in the annual precipitation: from 288 mm in 1984/85–1988/89 to 373 mm in 2003/04–2015/16. An increase in precipitation was noted during the ablation period; there was no significant increase in precipitation during the accumulation period. The rise in temperature could have led to a significant decrease in the proportion of solid precipitation in the lower part of the glacier in the summer. In addition, the increase in precipitation could be related to the relocation of the weather station. The unevenness of the precipitation curve after the relocation of the station was noted in a number of studies [*Kutuzov, Shahgedanova, 2009; Petrakov et al., 2016*].

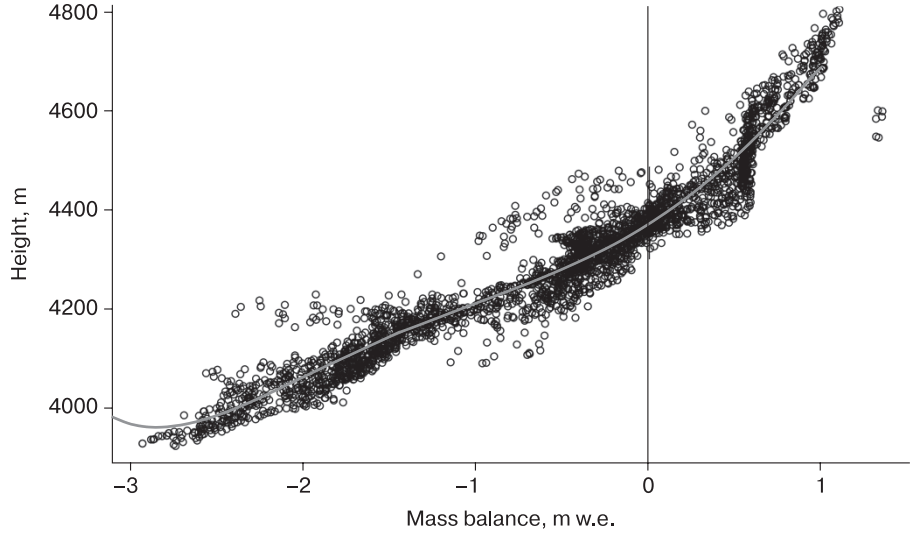

Fig. 10. Distribution of the annual mass balance depending on the absolute height according to the data of all grid cells of the model in 2014/15.

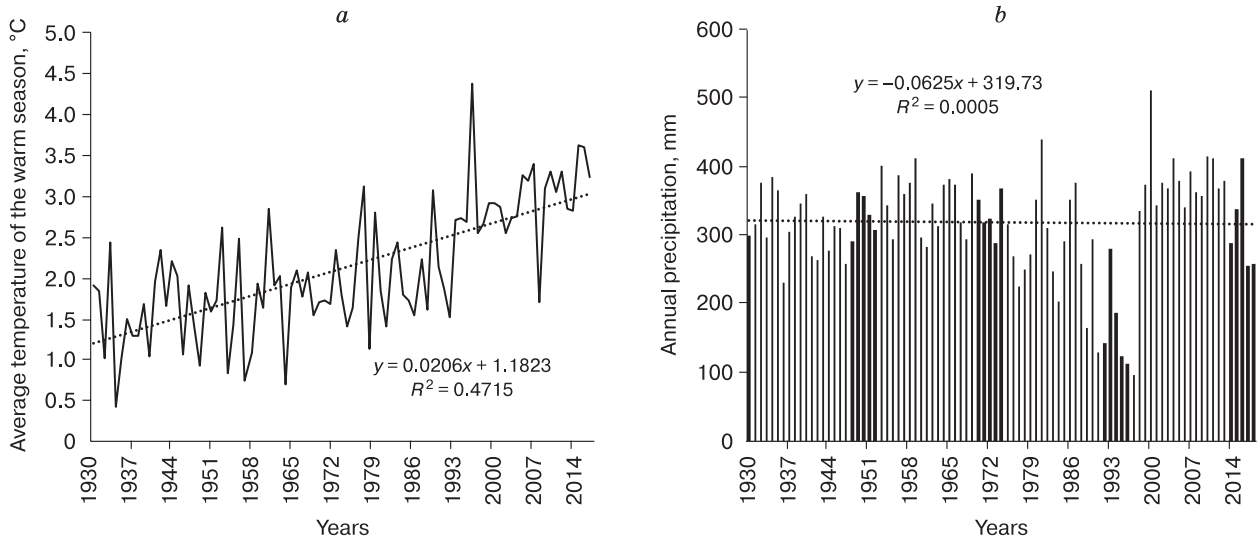

Fig. 11. Average air temperatures of the warm season (May–September) (*a*) and annual precipitation (*b*) according to the data of the Tien Shan and Kumtor weather stations for 1930–2018.

CONCLUSIONS

In this work, the physically based AMelt model of snow and ice melting in alpine zones was adapted to simulate the mass balance of glaciers under the climatic conditions of Central Asia. Approbation of an improved version of the model on the Sary-Tor Glacier for the period 2003/04 to 2015/16 demonstrated a good agreement with the results of glacial ablation measurements on a network of ablation stakes and the average subsidence of the glacier surface calculated using the geodetic method. The calibration coefficients (altitudinal gradient of temperature and precipitation) turned out to be close to the values observed in July–August 1984.

According to the modeling data, the annual accumulation values on the Sary-Tor Glacier in 2003/04–2015/16 varied within the range from 0.48 to 0.89 m w.e. and the ablation values, from –1.42 to –0.53 m w.e. The glacier mass balance was negative for most of the years during the study period and averaged –0.46 m w.e. per year. This value is significantly lower than the value observed in 1984–1989 (on average, –0.14 m w.e. per year). The ELA increased by 125 m: from 4225 in 1984/85–1988/89 to 4350 in 2003/04–2015/16. Such an intensification of mass loss is typical for all Tien Shan glaciers, on which mass balance observations have been performed.

According to modeling data, the dynamics of the mass balance of the Sary-Tor Glacier in the period from 2004 to 2016 repeats the trends noted for the Tien Shan glaciers according to direct observations and reconstructions by various authors. The obtained annual values of the mass balance are closest to the measured and modeled values characteristic of the nearby glaciers no. 354 and Western Suek. In general, according to the obtained results, the Sary-Tor Glacier is melting slower than the Urumqi and Tuyuksu glaciers to the east and faster than the Western Suek glacier.

Acknowledgments. *This work was supported by the grant of the President of the Russian Federation MK-2936.2019.5 in terms of modeling the mass balance of the Sary-Tor Glacier. The analysis of the problem of equifinality and the correspondence of the values of the calibrated parameters of the model to the observation data was supported by the Russian Foundation for Basic Research, project no. 20-35-70024. Selection and processing of remote sensing data and the analysis of the mass balance of the Tien Shan glaciers were carried out within the framework of state assignment no. AAAA-A16-116032810095-6. The analysis of long-term changes in the characteristics of the mass balance of the Sary-Tor Glacier was carried out within the framework of state assignment no. AAAA-A18-118022090056-0.*

The authors are grateful to the Kumtor Gold Company for providing meteorological data.

References

Aizen, V.B., Kuzmichenok, V.A., Surazakov, A.B., Aizen, E.M., 2007. Glacier changes in the Tien Shan as determined from topographic and remotely sensed data. Glob. and Planet. Change 56 (3–4), 328–340.

Armstrong, R.L., Rittger, K., Brodzik, M.J., et al., 2019. Runoff from glacier ice and seasonal snow in High Asia: separating melt water sources in river flow. Regional Environ. Change 19 (5), 1249–1261.

Ayala, A., Pellicciotti, F., Peleg, N., Burlando, P., 2017. Melt and surface sublimation across a glacier in a dry environment: Distributed energy-balance modelling of Juncal Norte Glacier, Chile. J. Glaciol. 63 (241), 803–822.

Barandun, M., Huss, M., Sold, L., et al., 2015. Re-analysis of seasonal mass balance at Abramov glacier 1968–2014. J. Glaciol. 61 (230), 1103–1117.

Barry, R.G., 2008. Mountain weather and climate. Cambridge Univ. Press, New York, 532 pp.

Belozerov, E., Rets, E., Petrakov, D., Popovnin, V., 2020. Modelling glaciers' melting in Central Caucasus (the Djankuat and Bashkara Glacier case study). E3S Web of Conferences, 163, p. 01002. EDP Sciences.

Beven, K., Freer, J., 2001. Equifinality, data assimilation, and uncertainty estimation in mechanistic modelling of complex environmental systems using the GLUE methodology. J. Hydrol. 249 (1–4), 11–29.

Bindi, M., Miglietta, F., Zipoli, G., 1992. Different methods for separating diffuse and direct components of solar radiation and their application in crops growth models. Clim. Res. 2, 47–54.

Bliss, A., Hock, R., Radić, V., 2014. Global response of glacier runoff to twenty-first century climate change. J. Geophys. Res. Earth Surf. 119 (4), 717–730.

Boland, J., Ridley, B., 2008. Models of diffuse solar fraction. In: Modeling Solar Radiation at the Earth's Surface. V. Badescu (Ed.). Springer, Berlin, Heidelberg, pp. 193–219.

Bolch, T., Shea, J.M., Liu, S., et al., 2019. Status and change of the cryosphere. In: The Extended Hindu Kush Himalaya Region. P. Wester, A. Mishra, A. Mukherji, A. Shrestha (Eds.). Springer, Cham., New York, pp. 209–255.

Carey, M., Molden, O.C., Rasmussen, M.B., et al., 2017. Impacts of glacier recession and declining meltwater on mountain. Societies, Ann. Amer. Assoc. Geogr. 107 (2), 350–359.

Christophersen, N., Neal, C., Hooper, R.P., et al., 1990. Modelling streamwater chemistry as a mixture of soilwater endmembers – a step towards second-generation acidification models. J. Hydrol. 116 (1–4), 307–320.

Coleou, C., Lesaffre, B., 1998. Irreducible water saturation in snow: experimental results in a cold laboratory. Ann. Glaciol., No. 26, 64–68.

DeWalle, D.R., Rango, A., 2008. Principles of snow hydrology. Cambridge Univ. Press, New York, 428 pp.

Dyurgerov. M.B., Kunakhovich, M.G., Mikhalenko, V.N., et al., 1992. Mass balance, runoff and meteorological conditions of the Sary-Tor glacier in the Ak-Shyirak ridge (Inner Tien Shan) 1985–1989. IGRAN, Moscow, 69 pp. (in Russian).

Dyurgerov, M.B. (Ed.), 1995. Glaciation of the Tien Shan. VINITI, Moscow, 237 pp. (in Russian).

Elagina, N., Kutuzov, S., Rets, E., et al., 2021. Mass balance of Austre Grønfjordbreen, Svalbard, 2006–2020, estimated by glaciological, geodetic and modeling approaches. Geosciences 11 (2), p. 78.

Garrick, M., Cunnane, C., Nash, J.E., 1978. A criterion of efficiency for rainfall-runoff models. J. Hydrol., No. 36, 375–381.

Huss, M., Hock, R., 2015. A new model for global glacier changes and sea-level rise. Front. Earth Sci., No. 3, p. 54.

Huss, M., Hock, R., 2018. Global-scale hydrological response to future glacier mass loss. Nat. Clim. Chang. 8 (2), 135–140.

Kaser, G., Grobhauser, M., Marzeion, B., 2010. Contribution potential of glaciers to water availability in different climate regimes. Proc. Natl. Acad. Sci. 107 (47), 20223–20227.

Kenzhebaev, R., Barandun, M., Kronenberg, M., et al., 2017. Mass balance observations and reconstruction for Batysh Sook Glacier, Tien Shan, from 2004 to 2016. Cold Reg. Sci. Technol., No. 135, 76–89.

Kirchner, J.W., 2006. Getting the right answers for the right reasons: Linking measurements, analyses, and models to advance the science of hydrology. Water Resources Res. 42 (3), W03S04.

Klok, E.L., Oerlemans, J., 2002. Model study of the spatial distribution of the energy and mass balance of Morteratschgletscher, Switzerland. J. Glaciol. 48 (163), 505–518.

Konovalov, V.G., 1985. Melting and runoff from glaciers in the river basins of Central Asia. Gidrometeoizdat, Leningrad, 239 pp. (in Russian).

Kronenberg, M., Barandun, M., Hoelzle, M., et al., 2016. Mass-balance reconstruction for Glacier No. 354, Tien Shan, from 2003 to 2014. Ann. Glaciol. 57 (71), 92–102.

Kutuzov, S., Shahgedanova, M., 2009. Glacier retreat and climatic variability in the eastern Terskey-Alatoo, inner Tien Shan between the middle of the 19th century and beginning of the 21st century. Glob. and Planet. Change 69, 59–70.

Kuzmin, P.P., 1961. The process of melting snow cover. Gidrometeoizdat, Leningrad, 364 pp. (in Russian).

Lehning, M., Völksch, I., Gustafsson, D., et al., 2006. ALPINE3D: a detailed model of mountain surface processes and its application to snow hydrology. Hydrol. Process. 20 (10), 2111–2128.

Lutz, A.F., Immerzeel, W.W., Gobiet, A., et al., 2013. Comparison of climate change signals in CMIP3 and CMIP5 multimodel ensembles and implications for Central Asian glaciers. Hydrol. Earth Syst. Sci., No. 17, 3661–3677.

McDowell, G., Huggel, C., Frey, H., et al., 2019. Adaptation action and research in glaciated mountain systems: Are they enough to meet the challenge of climate change? Glob. Environ. Change, No. 54, 19–30.

Mikhalenko, V.N., 1993. Calculation and reconstruction of the mass balance of the Ak-Shiyrak glacial system in the Tien Shan. Materialy Glaciol. Issled. [Data of Glaciological Studies], iss. 76, 102–107 (in Russian).

Narama, C., Kääb, A., Duishonakunov, M., Abdrakhmatov, K., 2010. Spatial variability of recent glacier area changes in the Tien Shan Mountains, Central Asia, using Corona (~1970), Landsat (~2000), and ALOS (~2007) satellite data. Glob. and Planet. Change 71 (1–2), 42–54.

Oerter, H., Moser, H., 1982. Water storage and drainage within the firn of a temperate glacier (Vernagtferner, Oetztal Alps, Austria). In: Hydrological Aspects of Alpine and High Mountain Areas: Proc. of the Exeter Symposium (July 1982, Exeter, UK), IAHS Publ., No. 138, pp. 71–83.

Petrakov, D., Shpuntova, A., Aleinikov, A., et al., 2016. Accelerated glacier shrinkage in the Ak-Shyirak massif, Inner Tien Shan, during 2003–2013. Sci. Total Environ., No. 562, 364–378.

Petrakov, D.A., Tutubalina, O.V., Shpuntova, A.M., et al., 2019. Assessment of glacier albedo in the Ak-Shiyrak massif (Inner Tien Shan) from ground-based and Landsat data. Earth's Cryosphere XXIII (3), 11–19.

Popovnin, V.V., Gubanov, A.S., Satylkanov, R.A., Ermenbaev, B.O., 2021. Reconstruction of the mass balance of the Sary-Tor glacier from meteorological data. Led i Sneg [Ice and Snow], 61 (1), 58–74 (in Russian).

Rets, E.P., Frolova, N.L., Popovnin, V.V., 2011. Modeling the melting of the surface of a mountain glacier. Led i Sneg [Ice and Snow], No. 4 (116), 24–31 (in Russian).

Rets, E., Kireeva, M., 2010. Hazardous hydrological processes in mountainous areas under the impact of recent climate change: case study of Terek River basin. In: Global Change: Facing Risks and Threats to Water Resources. Proc. of the Sixth World FRIEND Conf. Fez, IAHS Publ., Marocco, No. 340, pp. 126–134.

Rets, E.P., Kireeva, M.B., Loshakova, N.A., 2014. Heat balance model for the study of features formation of the flow of a glacial river (on example, of the r. Djankuat basin). Eurasian Union of Scientists (ESU), No. IV, 97–103 (in Russian).

Rohrer, M.B., Braun, L.N., 1994. Long-term records of snow cover water equivalent in the Swiss Alps, 2. Simulation. Nordic Hydrol. 25 (1–2), 65–78.

Rybak, O.O., Rybak, E.A., Yaitskaya, N.A., et al., 2019. Modeling the evolution of mountain glaciers: a case study of Sary-Tor glacier (Inner Tien Shan). Earth's Cryosphere XXIII (3), 27–42.

Semenova, O., Beven, K., 2015. Barriers to progress in distributed hydrological modelling. Hydrol. Processes 29 (8), 2074–2078.

Seo, D., Azar, A.E., Khanbilvardi, R., Powell, A., 2008. Analysis of snowpack properties and estimation of snow grain size using CLPX Data. Geosci. and Remote Sensing Symp., vol. 4, IV-1034–IV-1037.

Shannon, S., Smith, R., Wiltshire, A., et al., 2019. Global glacier volume projections under high-end climate change scenarios. Cryosphere, No. 13, 325–350.

Shea, J.M., Immerzeel, W.W., 2016. An assessment of basin-scale glaciological and hydrological sensitivities in the Hindu Kush-Himalaya. Ann. Glaciol. 57 (71), 308–318.

Shpuntova, A.M., Usubaliev, R.A., Petrakov, D.A., 2019. Modern changes in the area of glaciation of the Ak-Shyirak massif (Inner Tien Shan). In: Remote and ground-based studies of the Earth in Central Asia: Proc. of the Intern. conf. MoYuR Bishkek, Bishkek, pp. 252–258 (in Russian).

Siegfried, T., Bernauer, T., Guiennet, R., et al., 2012. Will climate change exacerbate water stress in Central Asia? Clim. Chang. 112, 881–899.

Singh, P., Singh, V.P., 2001. Snow and Glacier Hydrology. Kluwer Academic Publ., Boston, 742 pp.

Snow and Climate Physical Processes, Surface Energy Exchange and Modeling / R.L. Armstrong, E. Brun (Eds.), 2008. Antarctic Science. Cambridge Univ. Press, Cambridge, vol. 20 (6), pp. 610–611.

Sorg, A., Bolch, T., Stoffel, M., et al., 2012. Climate change impacts on glaciers and runoff in Tien Shan (Central Asia). Nat. Clim. Chang. 2 (10), 725–731.

Sorg, A., Huss, M., Rohrer, M., Stoffel, M., 2014. The days of plenty might soon be over in glacierized Central Asian catchments. Environ. Res. Lett. 9 (10), p. 104018.

Sturm, M., Holmgren, J., Konig, M., Morris, K., 1997. Thermal conductivity of seasonal snow. J. Glaciol. 43 (143), 26–41.

Takeuchi, N., Fujita, K., Aizen, V.B., et al., 2014. The disappearance of glaciers in the Tien Shan Mountains in Central Asia at the end of Pleistocene. Quatern. Sci. Rev. 103, 26–33.

Unger-Shayesteh, K., Vorogushyn, S., Farinotti, D., et al., 2013. What do we know about past changes in the water cycle of Central Asian headwaters? A review. Glob. and Planet. Change, 110, No. A, 4–25.

Ushnutsev, S.N., 1991. Oscillations of the mass balance of the Sary-Tor Glacier in the Inner Tien Shan and its reconstruction for 1930–1988. Materialy Glaciol. Issled. [Data of Glaciological Studies], iss. 71, 70–80 (in Russian).

Vinogradov, Yu.B., Vinogradova, T.A., 2010. Mathematical modeling in hydrology. Publisher. house "Academy", Moscow, 204 pp. (in Russian).

Voloshina, A.P., 1988. Climatic and meteorological features of the area of glaciation of the Ak-Shiyrak massif. Materialy Glaciol. Issled. [Data of Glaciological Studies], iss. 62, 184–193 (in Russian).

Zhupankhan, A., Tussupova, K., Berndtsson, R., 2017. Could changing power relationships lead to better water sharing in Central Asia? Water 9 (139), 17 pp.

URL: https://wgms.ch/ (last visited: 10.11.2019).

Received December 16, 2019
Revised May 8, 2021
Accepted June 20, 2021

Translated by A.V. Muravyov